ING Technical Note No. 123
Wavelength Dependent Pixel-to-Pixel Response Variations of a typical EEV42-80 CCD: the role of flat-fielding astronomical data.

Floris Crompvoets (Katholieke Universiteit Nijmegen, The Netherlands)*
Stephen Smartt (Isaac Newton Group, La Palma)

August 31, 1999

Abstract

High-quality, evenly illuminated images were taken at different optical wavelengths in order to determine how the photoresponse non-uniformity (PRNU) of an EEV42-80 Charge-Coupled-Device (CCD) depends on wavelength. The standard deviations of pixel values (in normalised frames) have been determined as a function of wavelength. This provides a measure of how the intrinsic pixel-to-pixel quantum efficiency (QE) variations of the device vary with incident photon colour. A summary of the main results includes:

1. The PRNU on large scales rises towards the blue end of the optical spectrum (<4000Å). By large scale we mean the cross-hatched diamond pattern (which is a characteristic of the EEV42-80's) and the behaviour of "bad-pixel" regions.
2. The severity of "bad pixel" troughs is a very strong function of incident wavelength especially in the blue.
3. The actual number of visibly bad pixels also increases dramatically towards the blue.
4. We estimate that the intrinsic small-scale pixel-pixel QE variations (on scales of $\sim$10$\times$10) in areas which are free from defective pixel clustering is $\sim$0.7%. With the statistical limits on the current data this appears constant from $\sim 3200 - 5700$Å (or at the very most it rises to $\sim$0.9% at the blue end).
5. We have monitored the PNRU over a period of one month, and find no evidence for temporal variations, within the statistical errors of our analysis.

We suggest that the standard method of flat-fielding CCD data will certainly remove the cosmetic non-uniformities, but that one should be very careful to use calibration frames which have the similar wavelength incident on each pixel as in the science frames, particularly with regard to removing the large-scale colour dependent PRNU. For example, if one wants to remove the bad-pixel defects to better than 1%, one should ensure that the wavelength of the flat-field light is within about 60Å of the target light falling on each pixel.

*Work carried out during student placement at ING during March-May 1999

1 Introduction

Modern Charge-Coupled-Devices (CCDs) are used at virtually every optical astronomical observatory, and provide the essential means of efficiently converting incident photons into astronomical computer images ([1]). Recent developments in CCD technology have produced devices which have very low intrinsic noise sources, such that they are usually shot-noise limited. A typical read out noise value for a device is in the region $2 - 5e^{-}$; hence for the lowest read-noise devices this noise source is close to negligible when the signal from the sky and source is greater than approximately 20 photons, and one is essentially shot-noise limited. This is almost always the case unless one is doing very high resolution spectroscopy or very high time-resolution monitoring. Thus in the shot-noise limited case, one is concerned with how much noise is introduced by individual pixel-pixel quantum efficiency variations. This is often referred to as photoresponse non-uniformity (PRNU). Normally, these variations are removed by dividing high-quality "flat-field" calibration frames into the astronomical images. The flat-fields are (relatively) evenly illuminated exposures with light of the same wavelength incident on each pixel as is incident from the target source. One naturally needs flat-fields of large enough counts such that shot-noise from the flats themselves is not introduced into the target frames. These frames should then reflect the real PRNU; however the magnitude of the intrinsic pixel-pixel variations and how this magnitude depends on wavelength has not been studied in detail for many CCDs on the market, and in particular the excellent new, thinned, devices from EEV (their EEV42-80 model).

A number of investigators have shared some unpublished results with us a comparison to what we are trying to quantify. For example Philips Research indicate that they do monitor the PRNU for each device that they sell, and for their largest format ($12\,\mu$ pixel) devices they measure typical values of 0.52% at 4500Å, 0.54% at 5500Å, and 0.61% at 6500Å. This is a surprisingly small variation over the 2000Å of spectral coverage that they observed ([2]), however these are frontsided chips which are more uniform than thinned ones. By comparison, Ken Smith provided results from an EEV CCD-26 (1353×286 frame transfer CCD) showing that the PRNU varied at 1.4% at 4000Å; 1.2% at 4500Å; 1.0% at 5500Å; 0.95% at 6500Å ([3]). This suggests a much larger wavelength dependent effect compared to what Philips have measured (however the Smith results are averaged over the whole CCD chip - an effect we will comment on later in this note). The devices that EEV release are quantified at 400, 6500 amd 9500Å (with a 800nm bandwidth), and their PRNU has generally been at the level of 1-2% over local regions of approximately 30×30 pixels. A brief experiment on the intra-pixel PRNU for an EEV42-80 CCD was carried out at the ATC in Edinburgh ([4]), and the results suggested that the PRNU could be as low as 0.25% at 6500Å (but over a small, single 6x6 pixel area on the chip).

Given the differences in the above results, and indeed the sparcity of serious detailed study, we have attempted to to shed some new light on this topic. The above summary suggests that comparing data from different sources is rather tricky given the difference in CCD types, and measurement and definition of the PRNU. We were also motivated by the universal question that astronomers and data reducers often ask about flat fielding methods and their impact on the final data product viz. would it be possible for an observatory to provide astronomers with a restricted library of very high quality master flat-field frames that they could use to calibrate their data for each CCD, rather than each obsever spending time taking their own specific data ? Hence we have taken high-quality flat-fields at different wavelengths and analysed these to determine the large and small scale PRNU as a function of the wavelength. We also investigated how the number and form of bad pixel regions varied with this wavelength.

2 The observing technique and reduction steps

Flat-field images were taken with the EEV12 CCD chip (EEV12 is the ING device label) on the blue arm of the ISIS spectrometer [1]. The CCD is a EEV42-80 type, science Grade 2 device. It has 4096×2048 physical pixels with two overscan regions: one from column 2049 to column 2148 and the other from line 4097 to line 4200. The square pixels have a width of 13.5 μm. The chip is optimised for observing at blue optical and UV wavelengths (∼3000Å-6500Å), and hence is thinned (approximately 15μ), backilluminated and has an excellent anti-reflective (AR) coating which peaks at ∼98% transmission at 4000Å.

To evenly illuminate the CCD, the light from a tungsten lamp was used. The tungsten reponse provides a black-body type continuous response from the near UV to the red - however as with all filament lamps it has a very red peak and its blue output is by comparison quite poor. The slitwidth of ISIS was set to an 'on-sky' value of 4.0 arcsec (891 μm); which projects to approximately 14 pixels on the detector. The H2400B grating we used has a dispersion of 0.11 Å/pixel, giving an unvignetted region on the chip covering a wavelength range of 378 Å. The flat mirror rather than the dichroic was inserted below the slit to illuminate the blue optical train of ISIS. The CCD chip was windowed and read out at standard speed in order to provide a gain of close to 1, and low read-noise (which is negligible anyway at the photon levels we are working at). The window covered the full range (lines 1 – 4200) in the spectral direction of the chip including the overscan region. In the spatial direction only columns 500 – 1500 were read out, as these covered more or less the full spectrometer slit length.

The flat-field images were taken at seven central wavelengths: 3300 Å, 3600 Å, 3900 Å, 4200 Å, 4700 Å, 5200 Å, 5700 Å. We did not investigate beyond 6000Å due to the complicating fringing effects. The exposure time was set such that the highest pixel value in each setting was not more than 60,000 ADU, hence avoiding non-linearity effects. The lamp current was increased from 1.5 A to 1.8 A for the three lowest wavelengths to get a reasonable ADU level in a shortish period of time. The exposure times, number of frames, lamp current and minimum and maximum photon count are shown in a Table 1 for each wavelength. The minimum and maximum values refer to the blue and red end of each setting respectively.

The flat-field images were processed in IRAF. First, the average bias level from the overscan region is substracted from the entire image. are trimmed to get rid of the vignetted regions which cover roughly rows 0 – 750 and 3370 – 4096. After this, the images taken at the same wavelength are combined with a suitable cosmic ray rejection algorithm turned on. Finally, the combined images are normalised by fitting cubic splines to them and dividing the images by their

[1] http://www.ing.iac.es/∼sjst/isis/isis_homepage.html

wavelength [Å]	exposure time [s]	frames	lamp current [A]	photoncount min – max
3300	300	4	1.8	20800 – 84000
3600	300	2	1.8	35600 – 85400
3900	60	5	1.8	36000 – 231000
4200	180	5	1.5	105000 – 281000
4700	60	5	1.5	135000 – 213000
5200	35	5	1.5	140000 – 153500
5700	35	5	1.5	163500 – 190000

Table 1: Exposure time, number of frames taken, lamp current and minimum and maximum ADU pixel values after adding all frames at each wavelength.

fits. The gain of the CCD is almost exactly 1.00, hence no conversion from ADU to real photon events needed to be done in order to ensure meaningful noise measurements.

3 Analyis of the results

The normalised images are shown in the Figures 1-7. The horizontal direction is the spectral direction in all images. To the left is blue, to the right is red. The spike showing up in the image centered at 3600Å (Figure 2) is an instrumental effect within the ISIS spectrometer.

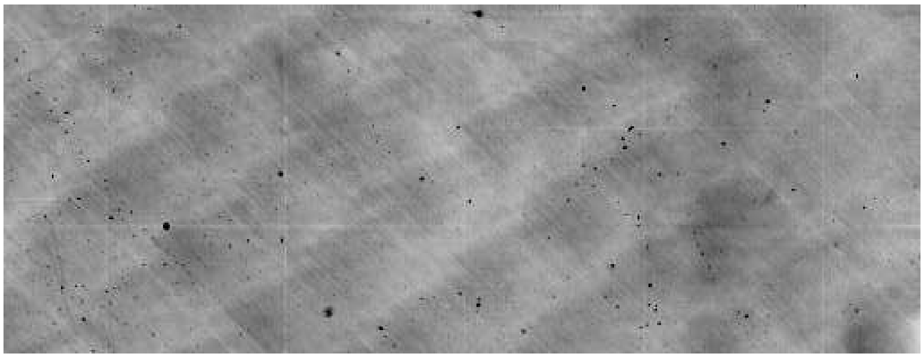

Figure 1: Normalised image centered at 3300 Å. The darker the region the lower the QE response is (similar colour scheme for all these images).

The "diamond" structure which is most distinct at the bluer wavelengths is an artefact of the CCD's backside process (and is a typical feature in EEV42-80's) as are the less distinct gridlines. This diamond structure causes a *large scale fluctuation* in the PRNU. This is shown for 3300 Å in Figure 8 and Figure 9. At this wavelength the fluctuation is largest, with a modulation about the normalised level of approximately ±2%.

At higher wavelengths broad ring-like structures are seen at the red end of the chip, these are only a fraction of a percent, and are probably due to dust specs on the CCD window. The more localized, deep spots on each image are

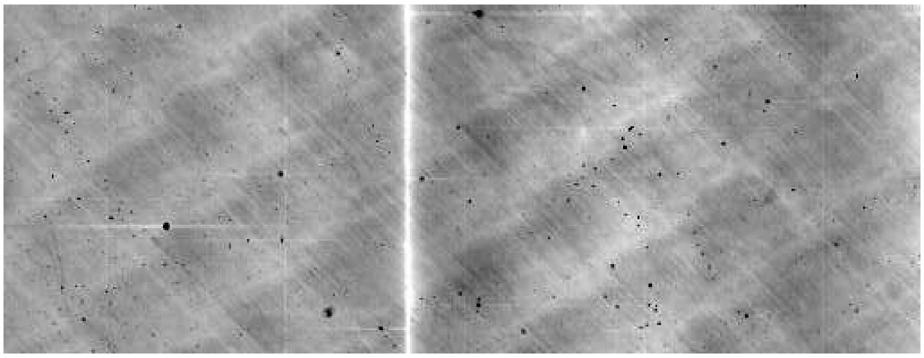

Figure 2: Normalised image centered at 3600 Å

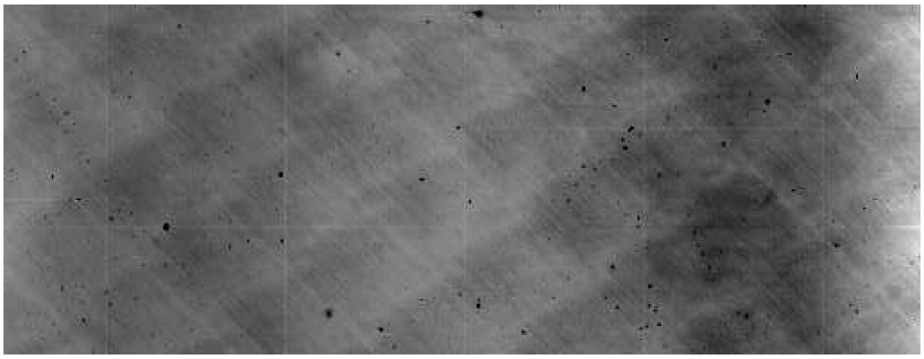

Figure 3: Normalised image centered at 3900 Å

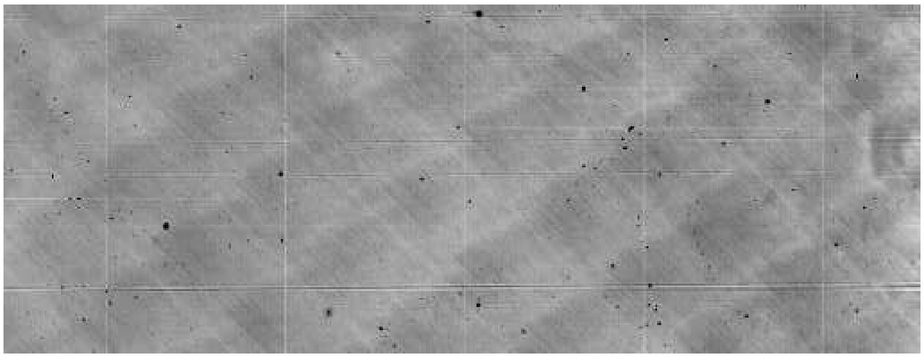

Figure 4: Normalised image centered at 4200 Å

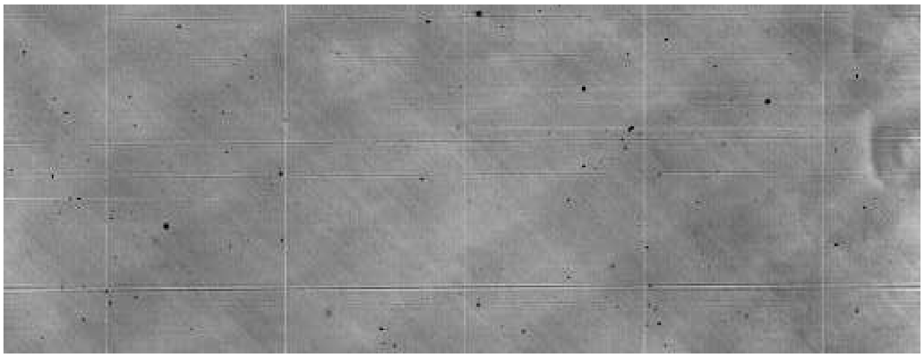

Figure 5: Normalised image centered at 4700 Å

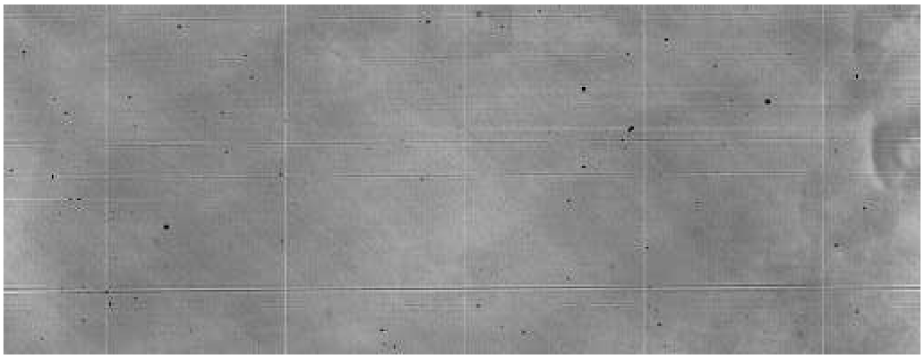

Figure 6: Normalised image centered at 5200 Å

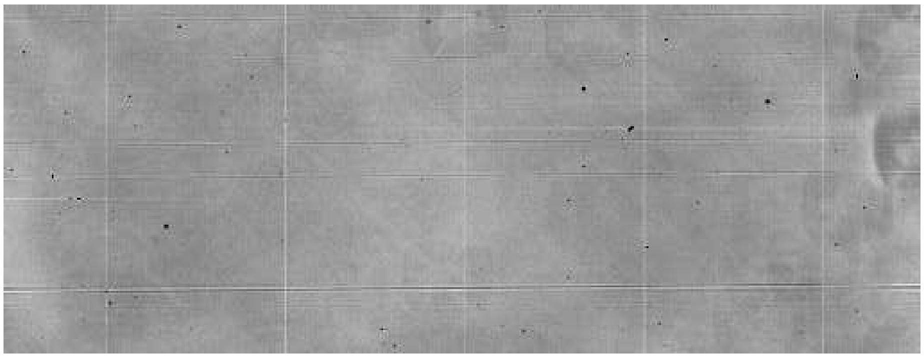

Figure 7: Normalised image centered at 5700 Å

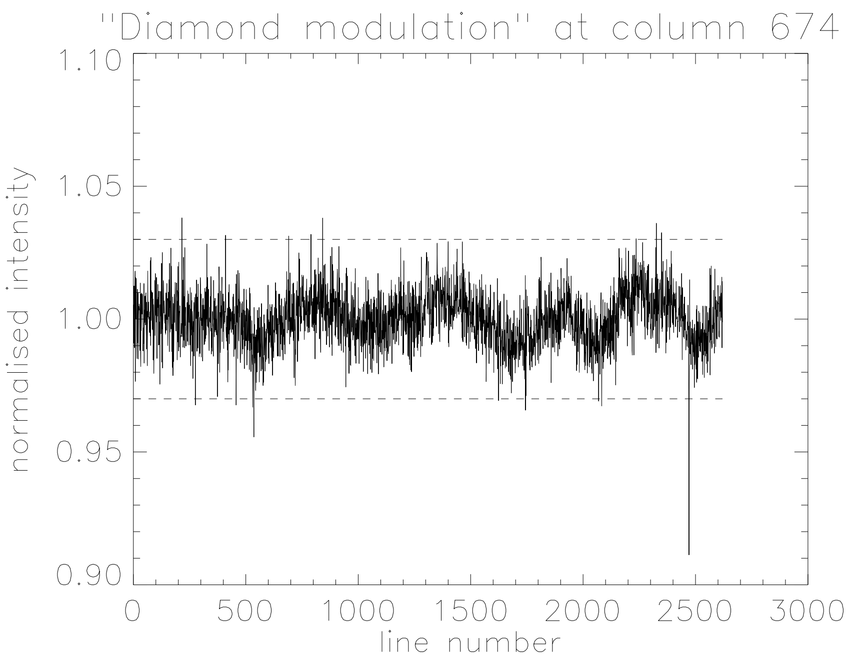

Figure 8: PRNU on a large scale due to the diamond structure. This is the variation along one column (spectral direction) of the CCD-chip.

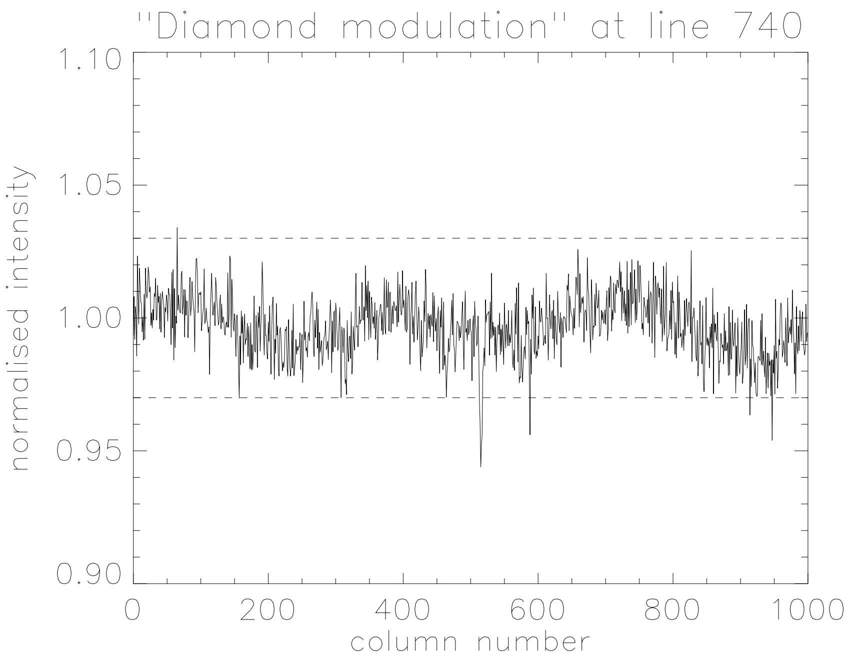

Figure 9: PRNU on a large scale due to the diamond structure. This is the variation along one line (spatial direction) of the CCD-chip.

bad pixel regions i.e. regions were the quantum efficiency drops dramatically. The existence of which is characteristic of all CCDs to some extent.

As a first attempt to quantify the PRNU in each frame, each normalised image was divided into strips of 50 rows width (in the spectral direction), and the full 1000 pixel height. The strips are thus composed of 50,000 pixels and the standard deviation in each strip was calculated. This is a measurement of the variation of pixel values, and as the frames were normalised it should hence be a measure of the variation of the pixel-pixel response, and hence the PRNU. This variation will also include a contribution from the photon shot noise; the magnitude of this noise factor is given by:

$$\sigma_{\text{noise}} = \frac{1}{\sqrt{N_{\text{signal}}}}. \tag{1}$$

Where N_{signal} is the total number of the photon counts. The range of N_{signal} at each wavelength setting is given in Table 1. Noise arising from other sources is very small and hence negligible (e.g the readnoise is 4e$^-$, and the thermal dark current is less than 0.7e$^-$ per hour).

The standard deviation measured in each of these 50×1000 pixel strips is shown in Figure 10 as a function of the wavelength of the light that is incident on the pixel strip.

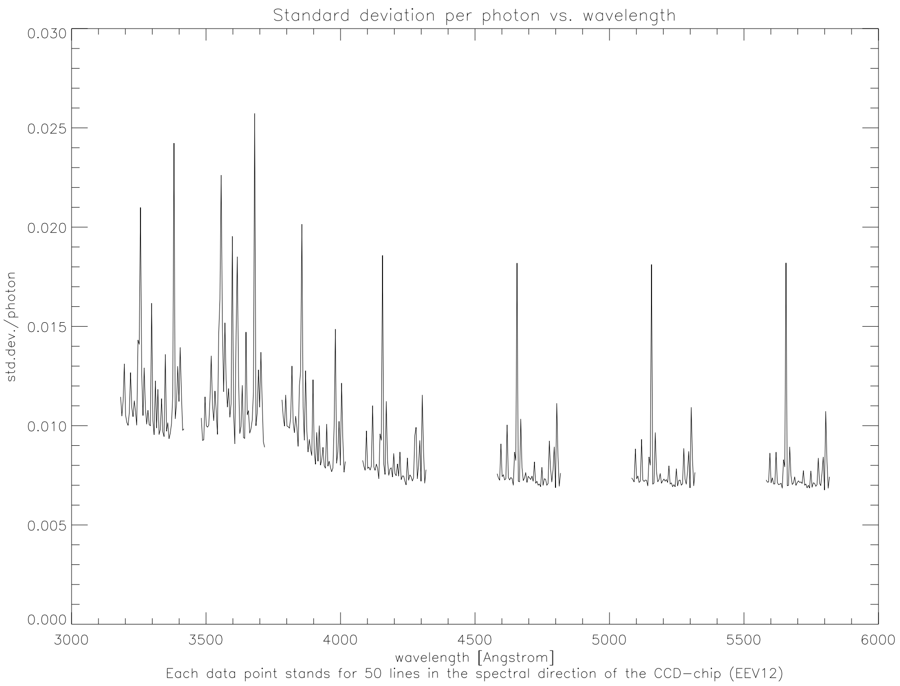

Figure 10: Normalised standard deviation as function of the wavelength. The standard deviation is calculated over strips which are 50 pixel columns by 1000 pixel rows

The plot in Figure 10 is divided into seven sections, were each corresponds to one wavelength setting of the CCD within the spectrometer. The standard deviation shows quite a striking, large scale, repetitive structure. This structure appears to increase towards the blue end of the spectrum. Looking at the normalised images in Figures 1-7 this is not surprising, as one can see the large scale structure (in terms of the bad pixel groups, and the diamond cross-hatch pattern) becoming more visible to the eye. This hence contributes to the repetitive structural 'spikes' seen in Figure 10. Interestingly the amount of structural noise appears to peak at the 3600Å setting; a point we will return to later.

In order to remove structure on this scale, and to determine the the intrinsic pixel-pixel PRNU variation on smaller scales we calculated the standard deviation over small square areas of 10×10 pixels. This was done by calculating the normalised standard deviation of each pixel and its neighbours in a 9×9 square around it. This yields 100 standard deviations, which are averaged to one standard deviation of the 10×10 pixels area. Ten of these areas are selected across the entire image at roughly equal steps, and avoiding areas with bad pixels. Bad pixels would introduce effects similar to the large scale structure shown in Fig. 11. These small scale standard deviations are shown in Figure 11 as the solid lines. We have also calculated the theoretical shot noise from the photon statistics associated with each 10×10 pixel area (from the Equation(1) above), and plot these as the lower dotted lines. One can see immediately that there is a source of noise greater than that introduced purely from the photon statistics: this is indeed the PRNU. We address the meaning of these relative values in the next section.

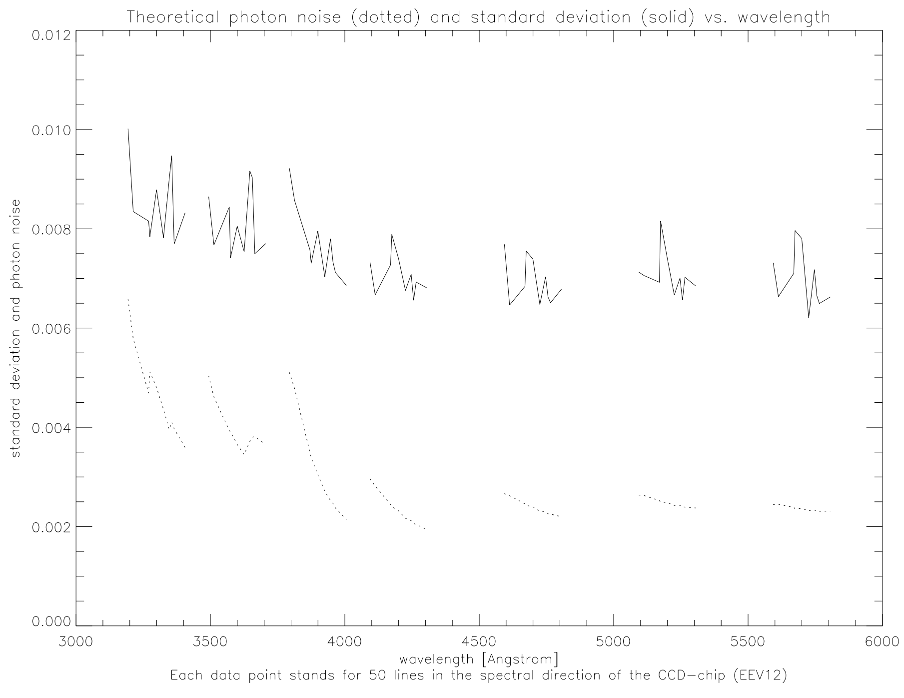

Figure 11: Normalised standard deviation as function of the wavelength. The standard deviation is calculated over small square areas of 10×10 pixels.

In order to determine how a region of bad pixels behaves when the incident wavelength changes we show 3D plots of normalised images in Figure 14 as a function of the central wavelengths. The bad pixel area is from column 60 to 210 and from line 735 to 805. In these plots the row axis is inverted and the real line numbers increase from left to right instead from right to left. One can easily see that the bad pixels' response is extremely wavelength dependent, and the severity of the effect increases sharply towards the blue. Again it appears that the worst case (i.e. when the central depths of the defective regions are at a minimum) occurs not at *the* bluest setting but at the central wavelength of 3600Å.

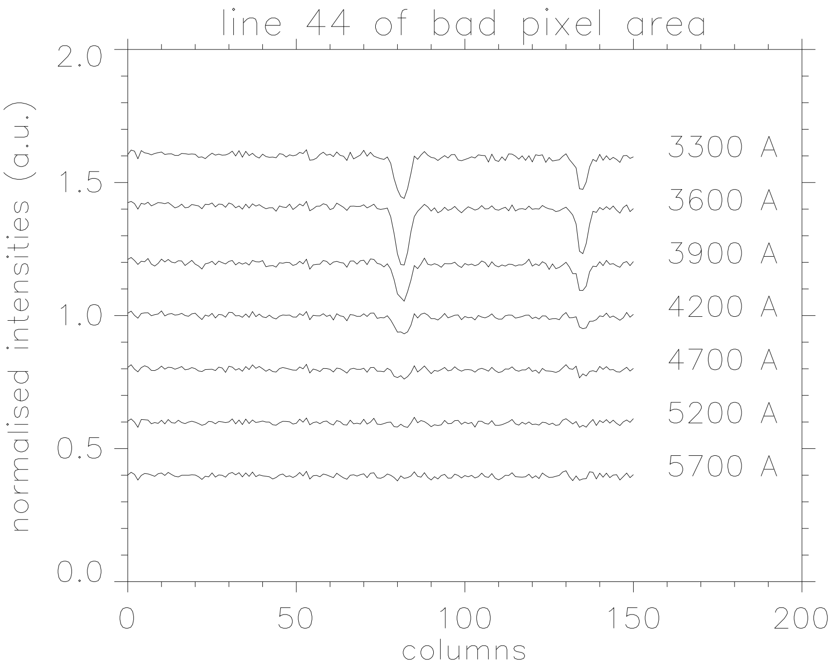

Figure 12: Line 44 of the bad pixel area for the different wavelengths. The different lines are given an offset.

In order to further illustrate the effect of bad-pixel severity as a function of wavelength we show a one-row cut through the bad pixel area at row 44 for each wavelength in Figure 12. Note that row 44 corresponds to line 26 in Figure 14 because of the inverted axis in this figure. This illustrates the obvious dependency on wavelength of the depth of the defective areas. In order to check if the general noise in the 'continuum' between the obvious depressions is of a fixed pattern (or has a contribution from a fixed pattern) which is in some way independent of wavelength we did the following test. We divided each wavelength setting by the 5700 frame, in an illustration of a typical flat-field calibration. Clearly the bad pixel regions still remain (in the frames 4700Å and bluer) at a similar level to the original frames, but from a qualitative comparison of the general PRNU in Figures 12& 13 it would appear that some of the fixed pattern contribution to the noise is removed. In Table 2 the RMS noise in line 44 is calculated (omitting the bad pixels values; columns 75 – 90 and 125 – 140) for each wavelength setting before and after the division by the 5700Å frame. In the last column we have calculated the theoretical photon noise resulting from

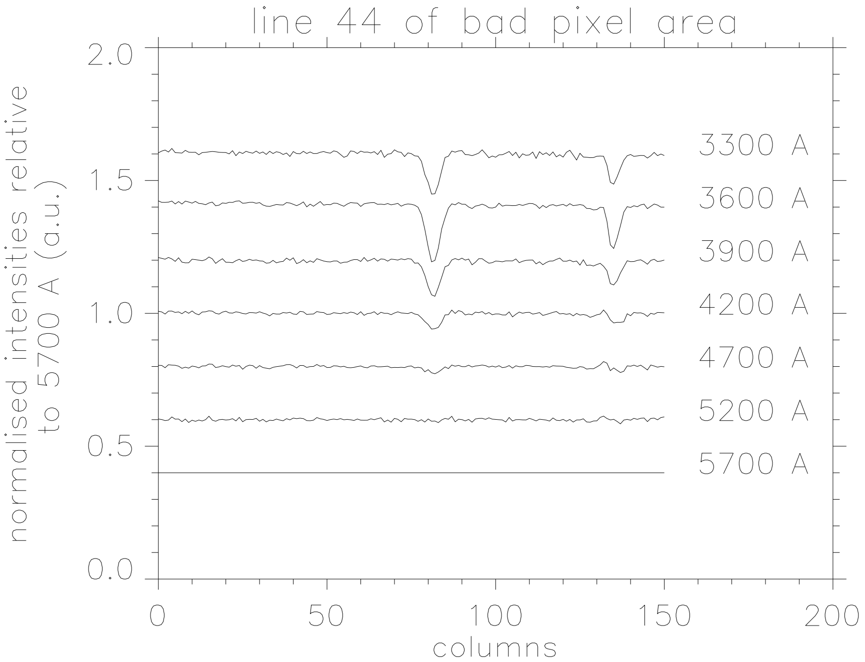

Figure 13: Line 44 of the bad pixel area. Each wavelength relative to 5700 Å. The different lines are given an offset.

the combination of two frames with 'perfect' Poisson photon statistics i.e. we calculate the combined noise as in Eqn(2), where N_{5700} is the number of counts in the 5700Å frame and N_λ is the number of counts in each of the others. One immediately notices that by flat-fielding each frame with the 5700Å image the measured RMS noise in this row is, in every case, decreased. This would suggest that there is a contribution from a fixed pattern PRNU which *to some extent* is wavelength *independent*. However it is obvious from Figure 13 that trying to calibrate out the PRNU from a science frame using one with different incident wavelength will not successfully remove the bad pixel defects.

$$\sigma_{\mathrm{comb.noise}} = \sqrt{\frac{1}{N_{5700}} + \frac{1}{N_\lambda}} \tag{2}$$

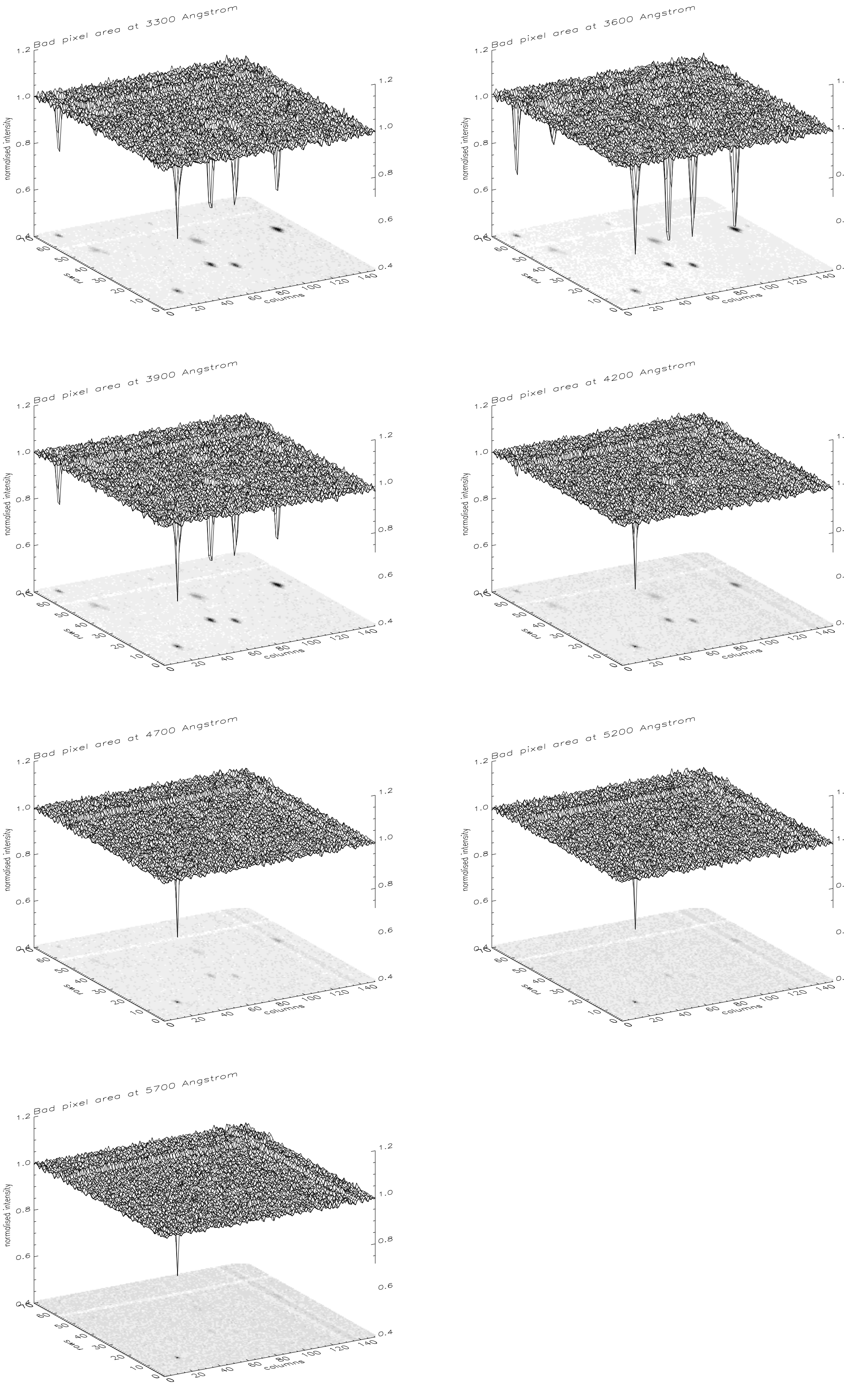

Figure 14: Bad pixel area, columns 60 – 210 and lines 735 – 805, are shown in a surface plot for the central wavelengths. Beneath the surface plot the real image is shown as well.

wavelength (Å)	RMS noise (%) before 5700Å division	RMS noise [%] after 5700Å division	Theoretical Combined Photon noise (%)
3300	1.1	0.79	0.62
3600	0.97	0.66	0.55
3900	0.89	0.63	0.51
4200	0.80	0.47	0.37
4700	0.71	0.40	0.36
5200	0.74	0.46	0.34
5700	0.74	–	–

Table 2: The RMS noise from line 44 of the bad pixel area for each wavelength both before and after division by the 5700Å frame.

4 Discussion of results and conclusions

In this technical note we have investigated how both the large scale and small scale PRNU (pixel-to-pixel noise variations) of an EEV42-80 depends on incident wavelength and also how this wavelength effects the behaviour and number of defective pixels. As flat-fielding with an evenly illuminated source is the technique normally used to calibrate out such characteristics, we will discuss our results within this context.

4.1 Large-scale PRNU variations

In the normalised combined flat-field images shown in Figures 1 – 7, the diamond structure is most distinct at lower wavelengths. From figures 8 and 9 we see that the large scale PRNU due to the diamond structure is less than 3 % at the shortest wavelength. However this structure is negligible at 5200Å, hence we have the trivial conclusion that over the wavelength region we have covered one could not use a single flat-field to calibrate out the large scale structure. One would have residuals up to 3%. The wavelength dependency of these large scale variations is consistent with the results in Figure 10. The obvious explanation of the diamond pattern is the blue response being more critically dependent on both the backside processing technique and surface structure anomalies. In back-illuminated CCDs the photons hit the silicon as their first barrier, within which they create an electron-hole pair. The detection of the photon is most efficient if the electron has a short distance to travel before it ends up in the depletion zone, otherwise this free electron may be captured by the p-type dopants and will not be detected. The absorption length in silicon at 4000Å is approximately 0.1μ (see Figure 15), hence virtually all of the photoelectrons are created very close to the silicon surface. Surface defects will hence critically effect the blue response of the CCD. The thickness variations of the chip may also clearly be a factor, as the electrons will have to pass through virtually the full silicon depth. For redder photons which are absorbed deeper into the silicon (e.g. 5700Å photons are absorbed at a depth of $\sim 5\mu$ - an absorption length 500 times larger than that for 3300Å photons) the thickness variations are less of an issue.

A similar explanation is probably valid for the strong dependence of the severity of the bad pixel troughs on wavelength (Figure 13). It is this strong dependence that explains the bluewards increase in number and intensity of the peaks in Figure 10. Bad pixel areas add a significant contribution (as well as the cross-hatch pattern) to the overall standard deviation in the 50 pixel wide strips. An interesting observation of the data presented in the images is that the very severe bad pixel areas at the lower wavelengths may exhibit a kind of charge blooming. One can see slightly raised intensity rows emanating from some of these regions (e.g. bottom left bad pixel region in Figure 1). Possibly charge leaks from these pixels along the rows, leaving them less full, and the row slightly enhanced in charge (however at a level lower than $\sim 1\%$). Another very interesting effect is that the severity of the bad pixel troughs appears to be worst at 3600Å rather than in the most extreme blue frame at 3300Å (see Figures 12 & 14). The simple interpretation of photon absorption

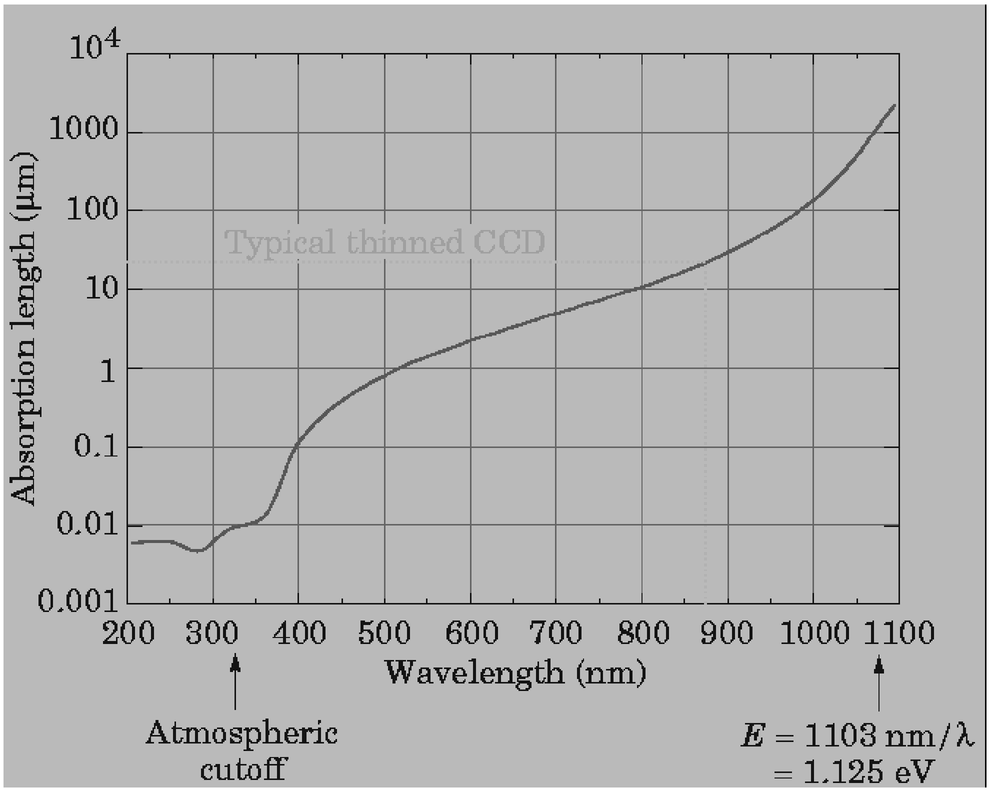

Figure 15: Photon absorption length of photons in silicon at 300K – from the excellent Web pages at the CCD development labs at UCO (http://gardiner2.ucolick.org/ ccdev/)

depth and surface/thickness dependency does not offer any explanation for this. Indeed we cannot offer any obvious physical reason, although we do note that in Figure 15 the absorption depth levels out sharply at approximately 3700Å, down to ∼3300Å. One possibility (Paul Jordon, private communication) is that the bluest photons which get trapped in the surface 'dead layer' may *have to* diffuse in order to be detected, which may tend to smooth out local variations. A test for this would be to carefully measure the MTF (e.g. by measuring widths of narrow projected arc lines) function of wavelength - if the above is indeed an explanation for the effect we see then the MTF should degrade rapidly towards 3300Å.

Most of the bad pixels in the normalised images have a normalised intensity around 0.9 but some have a much lower intensity, with the lowest being 0.09. So the sensitivity of this pixel is less than 10 % of the good pixels. Figure 14 shows how the bad pixels disappear at longer wavelengths. Only one very bad pixel remains. A cross section for line 44 of the bad pixel area (line 26 in Figure 14) is shown in Figure 12. Going from long wavelengths to short wavelengths the growth of the bad pixels can be seen. In Figure 13 the same is shown but now relative to the wavelength of 5700 Å. So there are less bad pixels at longer wavelengths.

4.2 Small-scale PRNU variations

To filter out the large-scale QE variations as we have just described, and to quantify the *intrinsic*, localised pixel-pixel PRNU we present the standard deviation vs. wavelength plot in Figure 11. The strong peaks are missing from this as we have taken 10 × 10 pixel boxes at 10 points across the chip, each of which were free of obviously defective areas.

In the frames 4200 – 5700Å we have data of high enough quality that the photon shot noise in these boxes is roughly constant at a level of 0.25%, as calculated from Eqn(1). In Figure 11 one can see that the measured standard deviation σ is quite constant in these four settings at ∼0.7%, significantly above the theoretical photon shot noise in each box. We interpret this as a measure of the intrinsic PRNU in the device i.e. the non-uniformity of the QE of individual pixels is in the region of 0.7% for incident light of 4200 – 5700Å. Below 4000 Å the measured standard deviation slowly rises to 0.8-0.9%, however because of the very red response of the tungsten lamp (and our limited access time to the spectrometer/telescope to carry out this experiment) we did not gather as many photons at the blue extreme. Hence the theoretical photon noise is also seen to rise towards the blue. The rise in the *measured* σ in Figure 11 bluewards of 4000Å can be totally accounted for purely by the decreasing photon statistics. Hence within the limits of our current measurements we can only say that the small scale, intrinsic PRNU is constant *magnitude* from 3200 – 5700Å at 0.7 ± 0.1%. This is quite a surprising result given that the obvious strong dependence on wavelength of the larger scale structures discussed in the previous section (the diamond pattern and the bad pixel dips). One interpretation of this is that the possible wavelength dependent surface defects and large-scale diamond structure (caused by the backside processing) are *only* present on the scale of 100's to 1000's of pixel areas, while the CCD is very uniform on small scales of 10's of pixels.

In support of this, in Table 2 and Figure 13 we show the results of trying to flat-field all the frames with the 5700Å exposure. We see the noise in the continuum (or the flat region free of pixel defects) is in all cases reduced by the flat-fielding attempt, however we could never reduce it to the photon shot noise limit. Also this was less successful in decreasing the PRNU noise in the bluer frames than those closer to 5700Å, as one would expect. Hence we conclude that although using flat-fields of different wavelengths would help to modulate the small-scale PRNU it does not remove it, and is less successful the further away one gets from the target wavelength. More critically the large scale structure is not removed, and it appears the best way to calibrate out these effects is indeed the tried and tested way of calibrating at each wavelength one is observing on sky.

Our numbers indicate that as the small-scale PRNU is of the order of $\sim$0.7%, then one should ideally aim for count-rates in the flat-fields of better than 0.3% so that noise from the photon statistics does not begin to introduce noise at a significant level. Hence for the EEV42-80's we recommend that observers who want to remove this 0.7% variation should get combined flat fields with over 100000 detected photons.

We were not able to fully repeat this experiment at a later date to check if the PRNU varied with time, however two series images at 3900Å were taken at approximately 1.5 month interval. The first was taken with the lamp current at 1.5A and the second at 1.8 A. The latter gave slightly higher quality flats though the images were very similar. The measured large and small scale standard deviations were similar and there was no differences between the bad pixel areas. We can conclude that over the 1.5 month interval we could not detect any change in the large or small scale PRNU, within the limits of our analysis.

The main conclusions from this note are summarized in the abstract. We are forced to conclude that creating a library of master-flats which would cover all observations with the EEV42-80 on this particular spectrometer (the blue arm of ISIS on the WHT) would be a very difficult task. Clearly one needs flats of wavelengths close to the observed to calibrate out the large scale effects of diamond cross-hatching and defective pixel areas. Using several fixed settings and *interpolating* between them is a possibility, however further tests would need to be carried out to see if this was much better than observers taking their own data. Also one would need to produce these flat-fields for every grating in ISIS, or else the interpolation would have to be in more than 2 dimensions. The later fact would complicate matters significantly, and allow room for errors in the processing. Hence, in this study alone, we unfortunately cannot recommend a better procedure for flat-fielding data (ISIS data in particular) than the observer carefully obtaining their required calibration data. Interpolation between very high-quality master-flats is a possibility, but would require further study.

Acknowledgments FMHC acknowledges support from ING for the 3 month student placement at ING, and support from an EC-Socrates programme between the universities of La Laguna and Utrecht. The authors thank Danny Lennon for taking some fine images, and advice over the course of the project.

References

[1] C. Buil, *CCD Astronomy*, Willmann-Bell, Inc., 1991.

[2] A. Theuwissen, Communication in CCD-World mail listings, 1999

[3] K. Smith, Communication in CCD-World mail listings, 1999

[4] S. Tulloch, The measurement of spatial resolution in EEV42-80 CCD images, *RGO Technical Note 118*, 1998